

## Low-lying structure of light radon isotopes

D. J. Dobson,<sup>1</sup> S. J. Freeman,<sup>1,\*</sup> P. T. Greenlees,<sup>2</sup> A. N. Qadir,<sup>1</sup> S. Juutinen,<sup>2</sup> J. L. Durell,<sup>1</sup> T. Enqvist,<sup>2</sup> P. Jones,<sup>2</sup> R. Julin,<sup>2</sup>  
 A. Keenan,<sup>2</sup> H. Kettunen,<sup>2</sup> P. Kuusiniemi,<sup>2</sup> M. Leino,<sup>2</sup> P. Nieminen,<sup>2</sup> P. Rakkila,<sup>2</sup> S. D. Robinson,<sup>1</sup> J. Uusitalo,<sup>2</sup>  
 and B. J. Varley<sup>1</sup>

<sup>1</sup>*Schuster Laboratory, University of Manchester, Manchester M13 9PL, United Kingdom*

<sup>2</sup>*Department of Physics, University of Jyväskylä, Jyväskylä, Finland*

(Received 19 September 2002; published 31 December 2002)

The excited states in the neutron-deficient isotopes  $^{200,202,204}\text{Rn}$  have been populated using the  $^{168}\text{Er}(^{36}\text{Ar},4n)$ ,  $^{166}\text{Er}(^{40}\text{Ar},4n)$ , and  $^{168}\text{Er}(^{40}\text{Ar},4n)$  reactions at beam energies of 175, 182, and 177 MeV, respectively. Evaporation residues were selected using an in-flight gas-filled separator and implanted at the focal plane into a 16-element position-sensitive, passivated ion-implanted planar silicon detector. Prompt  $\gamma$  rays were observed at the target position using an array of Compton-suppressed germanium detectors. Correlation with the subsequent radioactive decay of associated recoiling ions in the silicon detector, recoil- $\gamma$  and recoil- $\gamma$ - $\gamma$  coincidences were used to construct decay schemes of light radon isotopes. Measurements of delayed  $\gamma$  rays at the focal plane have also been made, and microsecond isomers have been observed in  $^{200,202}\text{Rn}$ , but not in  $^{204}\text{Rn}$ . Comparison of the results with those for polonium isotopes indicate a common mechanism for the onset of deformation. Candidates have been found in  $^{202,204}\text{Rn}$  for deformed intruder states which coexist with the spherical ground-state shape.

DOI: 10.1103/PhysRevC.66.064321

PACS number(s): 27.80.+w, 23.20.Lv, 23.60.+e, 25.70.Gh

### I. INTRODUCTION

In several regions of the periodic table, the onset of deformation has been associated with the presence of deformed particle-hole intruder configurations coexisting with spherical ground-state shapes. These intruder configurations occur at low excitation energy due to a gain in the total pairing energy. They fall in excitation energy with increasing numbers of valence particles due to an increase in the total proton-neutron interaction energy [1], eventually falling lower in energy than the spherical configurations, at which point the ground state assumes a large permanent deformation. Spherical and deformed configurations may mix before this point is reached, introducing admixtures of the deformed configuration into the ground and low-lying states.

Over the past few years there have been extensive measurements of excited  $0^+$  states and associated bands in even-even lead, mercury and platinum isotopes with  $N < 126$  [1,2]. They have been interpreted in terms of intruder states based on proton particle-hole excitations across the  $Z=82$  shell gap. In some cases, excited levels based on these states have been observed which correspond to deformed rotational bands, and supporting evidence has been obtained through the measurement of transition probabilities. Similar particle-hole intruder states should be present in nuclei above the  $Z=82$  closure, such as  $4p2h$  and  $6p2h$  configurations in the polonium and radon isotopes. Low-lying  $0^+$  states in polonium isotopes have been observed in the  $\alpha$  decay of  $^{200,202}\text{Rn}$  [3,4] and in the  $\beta$  decay of  $^{200,202}\text{At}$  [5,6]. Energy systematics and branching ratios have been used to interpret such states as intruders which appear to mix with the spherical ground-state configurations in isotopes lighter than  $^{200}\text{Po}$ . In addition, in-beam  $\gamma$ -ray studies of  $^{196,198}\text{Po}$  [7,8] have found

$2_2^+$  and  $4_2^+$  states which have been associated with rotational bands built on top of the intruding  $0^+$  states. Studies of low-lying yrast states in lighter isotopes [9] indicate that there is strong mixing of deformed intruders and spherical ground-state configurations in  $^{194}\text{Po}$ , while the intruder configurations dominate in the ground state of  $^{192}\text{Po}$ . Alternative interpretations of the observed  $2_2^+$  and  $4_2^+$  states in terms of anharmonic vibrations [10] are inconsistent with recent calculations [11], which cannot reproduce the observed changes in the lighter isotopes with physically meaningful parameters in a particle-core model.

This paper presents an investigation into the structure of neutron-deficient radon isotopes. A consistent picture of the onset of deformation around  $Z=82$  would predict effects in the radon isotopic chain similar to those observed in polonium isotopes, namely, a transition from spherical vibrational characteristics to deformed systems with the fall in excitation energy of intruder configurations with increasing neutron deficiency. Long-standing macroscopic-microscopic models [12–15] have predicted that deformed ground-state shapes exist beyond  $^{202}\text{Rn}$ . The existing results in radon isotopes lighter than  $^{204}\text{Rn}$  are confined to the first few yrast excited states [16–18], ending in the most neutron-deficient isotope with known excited levels  $^{198}\text{Rn}$ . A steep fall in the excitation energy of  $J=2^+$  and  $4^+$  states beyond  $A=204$  is suggestive of the spherical  $\pi h_{9/2}^4$  structures close to  $A=212$  being crossed by states whose structure is quite different and which become energetically favored with increasing numbers of neutron holes. Such systematics of just a few states can often look somewhat misleading as mixing of deformed and spherical configurations may shift the energies of the lowest lying states away from simple expectations. A study was therefore undertaken to establish states at higher spins in order to clarify the issue and to search for candidates for coexisting intruder configurations.

\*Email address: sjf@mags.ph.man.ac.uk

## II. EXPERIMENTAL DETAILS

The three isotopes studied were all produced using  $4n$  evaporation channels following the fusion of Ar beams with Er targets. The production cross sections for the evaporation residues range from around 1 mb, in the case of  $^{204}\text{Rn}$ , down to around  $1\ \mu\text{b}$  for the lightest isotope studied, whilst the total fusion cross section is of the order of 100 mb. Techniques are therefore necessary to isolate the in-beam  $\gamma$  rays emitted by evaporation residues surviving fission from radiation associated with the profusion of fission fragments produced concomitantly. To exacerbate the problem, strong Coulomb excitation of the target nuclei occurs. In addition to the issue of selection of the desired events from those associated with these backgrounds, in the case of submillibarn production cross sections the issue of isotopic identification is important. Where there is sufficient data to allow coincident  $\gamma$ - $\gamma$  analysis to be performed, new transitions may be associated with known transitions in a particular isotope. But where only singles events are available, new transitions must be positively identified with the emitting nuclide, even when low-lying transitions are already known.

Three different reactions were used in this study. Excited states in  $^{200}\text{Rn}$  were populated in the  $^{168}\text{Er}(^{36}\text{Ar},4n)$  reaction. A self-supporting metallic target, of thickness  $500\ \mu\text{g cm}^{-2}$  and highly enriched in  $^{168}\text{Er}$ , was bombarded with a beam of  $^{36}\text{Ar}^{7+}$  ions at an energy of 175 MeV, delivered by the K-130 cyclotron at the Accelerator Laboratory of the University of Jyväskylä. The same machine was used to supply a beam of  $^{40}\text{Ar}^{8+}$  ions at 182 MeV to initiate the  $^{166}\text{Er}(^{40}\text{Ar},4n)$  reaction producing excited states in  $^{202}\text{Rn}$ , using similar target properties. The final reaction reported here used the same beam at an energy of 177 MeV in a study of  $^{204}\text{Rn}$  using the reaction  $^{168}\text{Er}(^{40}\text{Ar},4n)$ .

The basic experimental equipment was similar for all experiments. Recoiling evaporation residues were separated from primary beam particles, fission fragments and other reaction products using the high-efficiency, gas-filled recoil separator RITU [19]. This was filled with He gas at a pressure of 1 mbar and isolated from the accelerator vacuum by a thin carbon foil of thickness  $\sim 50\ \mu\text{g cm}^{-2}$  upstream of the target position. At the focal plane of RITU, separated ions were stopped in a position-sensitive passivated ion-implanted planar silicon detector. This detector was 35 mm high and 80 mm wide with a thickness of  $300\ \mu\text{m}$  and covered approximately 70% of the recoil distribution at the focal plane. The width was subdivided into 16 strips, each 5 mm wide. Vertical position along these strips was obtained on the basis of resistive division between signals taken from the top and the bottom of each strip. A summed signal was also recorded giving the energy deposited. Energy and position signals were recorded for events corresponding to the implantation of recoiling ions into the silicon detector and for their subsequent  $\alpha$  decays. Two sets of amplifiers were used, one with low gain suitable for the energies associated with the recoiling ions (10–40 MeV) and another with high gain suitable for  $\alpha$ -particle energies (6–8 MeV). Events in the silicon detector due to  $\alpha$  decay and implantation of recoiling ions were primarily distinguished on the basis of the re-

corded energy signal. Further selection was provided by a multiwire gas-filled parallel-plate avalanche counter which was placed 20 mm in front of the silicon detector. The two sorts of events were distinguished in terms of the presence or absence of a coincidence between gas and silicon detectors. Residual scattered beam and other reaction products reaching the focal plane were differentiated from recoiling fused ions on the basis of a time-of-flight measurement through RITU. A large area silicon counter composed of four separate quadrants was placed behind the position-sensitive detector. This was used to veto events which appear to be connected with very energetic light particles punching through the position-sensitive detector which would otherwise contribute to the background in  $\alpha$ -particle energy spectra. In the  $^{202}\text{Rn}$  experiment, a second gas detector was situated at a distance  $\sim 310$  mm upstream from the first, allowing a time-of-flight measurement between the two gas counters to be made giving further discrimination between recoiling ions and residual scattered beam particles.

Prompt electromagnetic radiation emitted at the target position was detected in the JUROSPHERE array. This array consisted of a number of different types of Compton-suppressed germanium detectors arranged in five rings around the target position. The general arrangement of these three sorts of detector was as follows: fifteen EUROGAM phase I detectors of 70% nominal efficiency [20] (ten at  $134^\circ$  to the beam direction and five at  $158^\circ$ ), seven 25%-efficient TESSA detectors [21] (five at  $101^\circ$  and two at  $63^\circ$ ), and five NORDBALL detectors [22] with efficiencies that range between 25 and 40% at  $79^\circ$ . There were minor changes in this general arrangement for each experiment, but the measured absolute efficiency of the setups used was close to 1.7% at 1332 keV in each case.

Delayed electromagnetic radiation emitted at the focal plane of RITU was also detected using Compton-suppressed germanium detectors. In the  $^{200}\text{Rn}$  experiments a single NORDBALL detector was used in close geometry with the position-sensitive silicon detector. During the  $^{202}\text{Rn}$  experiment, further detectors were added to give a total of three suppressed NORDBALL detectors and one unsuppressed EUROGAM detector for the second half of the duration of the experiment. For the  $^{204}\text{Rn}$  experiment, four suppressed NORDBALL detectors and one unsuppressed EUROGAM detector were used. The  $^{200}\text{Rn}$  experiment was repeated without the target position array, but with the same focal plane setup as  $^{204}\text{Rn}$ , in order to improve information on isomeric decays.

Timing information for various detectors were recorded in several ways. Individual germanium times were recorded relative to the cyclotron RF signal and also relative to the arrival of a recoil at the focal plane. A generic prompt recoil- $\gamma$  time interval was recorded between the arrival of a recoil and the firing of any target position germanium detector. A similar delayed recoil- $\gamma$  interval was generated for focal plane germanium detectors. Coincidence  $\gamma$ - $\gamma$  timing was recorded for both target and focal plane detectors between the logical definitions of a  $\gamma$ - $\gamma$  event and any  $\gamma$  in the signal processing. For the  $^{202}\text{Rn}$  experiment, a second time-of-flight

measurement between the two gas counters was also recorded.

The data acquisition was triggered by an event in the position-sensitive silicon detector at the focal plane. On satisfying this trigger, 6  $\mu$ s gates were opened to receive any prompt signals from focal-plane Si and gas detectors, and target-position germanium detectors, along with the relevant timing information. In addition, longer 32  $\mu$ s gates were opened for any delayed isomeric  $\gamma$  decays measured in the focal plane germanium detectors. Along with these event parameters, the absolute time of event trigger generation was recorded to a precision of 1  $\mu$ s by a 1 MHz scaler which ran continuously for the duration of each experiment. This provides information so that temporal correlations between pairs of events can be built up during off-line sorting of the event data.

Data were collected in each experiment for approximately five days with beam currents typically of the order of 10 pnA, limited by the rate in the target-position germanium detectors, around 5–6 kHz Compton-suppressed rate per 70% detector. Under these conditions the position-sensitive silicon detector counted at rates of 20–30 Hz.

### III. DATA REDUCTION AND ANALYSIS

Two approaches have been used in the data analysis of the current work. Where possible, recoil- $\gamma$ - $\gamma$  coincidence measurements have been used to build up level schemes, as in  $^{202,204}\text{Rn}$ , using known low-lying transition energies. Yield of data for  $^{200}\text{Rn}$  was lower and new  $\gamma$ -ray transitions are not easily associated with known transitions between low-lying states using coincidence measurements; a problem of identification thus arises. Identification of new transitions in this case was performed by correlation of recoil- $\gamma$  events with the subsequent radioactive  $\alpha$  decay of the recoil measured at the same position in the silicon detector.

The germanium detectors were matched in terms of energy using singles spectra taken using  $^{152}\text{Eu}$  and  $^{133}\text{Ba}$  sources. These were used to obtain gain matching coefficients and to produce a relative efficiency calibration for the target-position detectors. Doppler-shift corrections were made to the in-beam  $\gamma$ -ray data using calculated values of the recoil velocity in each case. For  $^{202,204}\text{Rn}$ ,  $\gamma$ - $\gamma$  matrices were produced from the event data subject to constraints on recoil- $\gamma$  and  $\gamma$ - $\gamma$  timing measurements to minimize time-random backgrounds.

In order to establish sequences of correlated events for the  $^{200}\text{Rn}$  experiment, further data manipulation is required. These techniques, summarized here, are identical to the previous study of  $^{198}\text{Rn}$  [18] and the reader is referred to that reference for further details. A small linear dependence of the measured  $\alpha$  energies with position along the strips in the silicon detector is corrected via an appropriate transformation. Individual strips were then gain matched and added together. An internal calibration was performed on the resulting spectrum using known  $\alpha$ -particle energies in order to confirm the identification of decays in the energy spectrum. To effectively correlate positions of recoil and decay events, the position measurements derived from the two respective

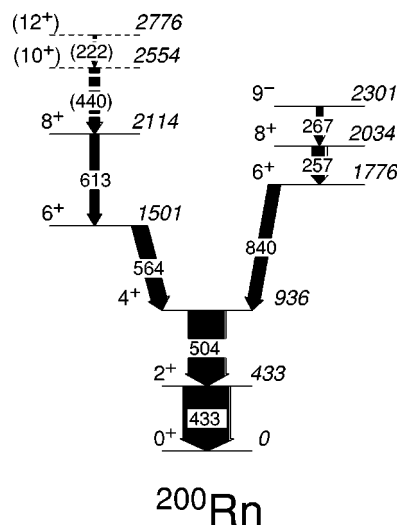


FIG. 1. The level scheme for  $^{200}\text{Rn}$  deduced from measurements of the  $^{168}\text{Er}(^{36}\text{Ar},4n)$  reaction. Transitions are labeled with the transition energy to the nearest keV. Excited states are labeled by the assigned spin parity and excitation energy in keV. Tentative placements are shown with dashed lines.

banks of amplifiers were matched using short-lived isotopes produced in the reaction. Recoil- $\alpha$  correlations were established by searching through the data to find the  $\alpha$  decay corresponding to implantation at a particular position in the silicon detector. The energy of the  $\alpha$  decay and the half-life uniquely define the isotopic character of recoiling ion. Prompt  $\gamma$ -ray transitions measured at the target position, in coincidence with that recoil, are then also associated with that isotope.

In correlation analysis it is essential for the mean lifetime of the isotope of interest to be small in comparison with the average time between two implantations at a particular position in the detector. For the detector as a whole the latter was measured to be 24 s, but varied between 13 s in the center to 64 s at the edges of the recoil distribution. Given that the known half-life of  $^{200}\text{Rn}$  is 1.06(2) s [23], good correlation conditions should be expected. Subsequent implantation at the same position and the escape of  $\alpha$  particles from the detector put restrictions on the maximum length of time after an implantation that the decay can be searched for. A search time of 5 s was chosen. It is also instructive to vary this search time in order to identify any possible contaminant  $\gamma$ -ray transitions arising from bad correlations.

## IV. RESULTS

### A. Level scheme of $^{200}\text{Rn}$

A previous in-beam study of  $^{200}\text{Rn}$ , using radioactive-decay correlations, established two low-lying transitions in the decay scheme which were assumed to be the  $4_1^+ \rightarrow 2_1^+$  and  $2_1^+ \rightarrow 0_{g.s.}^+$  transitions with energies of 504.3(2) and 432.9(2) keV, respectively [17]. The current work extends the level scheme up to spins of  $\sim 12\hbar$  and the resulting level scheme is shown in Fig. 1. The current work also provides

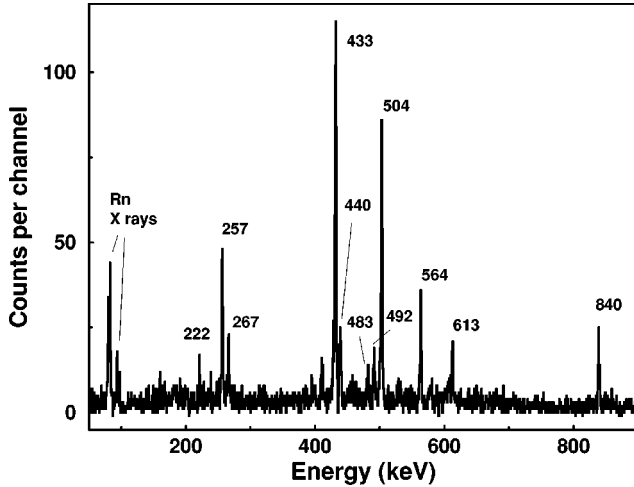


FIG. 2. Energy spectrum of prompt  $\gamma$  rays emitted at the target position by ions which subsequently  $\alpha$  decay at the focal plane with characteristics which are associated with  $^{200}\text{Rn}$ . Strong peaks are labeled by the transition energy in keV.

evidence for the spin assignments and for a previously unobserved isomer.

The  $\alpha$ -particle energy spectrum at the focal plane indicates that the variety and yield of the isotopes produced is similar to that observed in the  $^{176}\text{Hf}(^{28}\text{Si},4n)$  reaction used previously [17]. Assuming the transmission through the separator is 25% and an  $\alpha$ -particle detection efficiency limited to 50% by escape events, the  $\alpha$ -particle yields indicate an estimated cross section of  $4 \mu\text{b}$ . Figure 2 shows the prompt  $\gamma$ -ray spectrum, after time-random subtraction, associated with  $^{200}\text{Rn}$  recoil- $\alpha$  correlations. The effect of changing the correlation search time was investigated and all the transitions in the spectrum scale in the manner expected for a half-life of the order of 1 s. These transitions are therefore all assigned to  $^{200}\text{Rn}$ , the energies and relative intensities of which are listed in Table I.

The use of full  $\gamma$ - $\gamma$  coincidence techniques is not viable in the case of  $^{200}\text{Rn}$  due to lack of statistics. Some coincidences can be verified in a recoil- $\alpha$  correlated  $\gamma$ - $\gamma$  matrix, but with such low statistics the nonobservation of a transition in a gated spectrum is not significant and such techniques are therefore limited. In general the decay sequences have to be ordered on the basis of relative intensity, with the help of the decay pattern of an isomeric state discussed below.

In order to assign spin changes angular distributions of  $\gamma$ -ray intensity were investigated. Given that in order to observe  $\gamma$  rays from  $^{200}\text{Rn}$  recoil-decay correlation is necessary and that the range in angles is rather limited, full angular distribution analysis is not possible. Instead simple three point distributions were performed. Decay-correlated prompt  $\gamma$ -ray data were incremented as a function of angle. The data from the  $79^\circ$  and  $101^\circ$  detectors were combined to produce a single data point in  $\cos\theta$  with similar statistical significance to the  $134^\circ$  and  $158^\circ$  angles, where the larger, more efficient detectors were placed. Angle-to-angle normalizations were derived from data taken with radioactive sources. The resulting distributions are shown in Fig. 3, where most low-lying

TABLE I. Energies and deduced spins of excited states in  $^{200}\text{Rn}$ . Measured transition energies and relative intensities of de-exciting  $\gamma$  rays are listed along with the inferred multiplicities. Relative intensities of transitions are listed and have been corrected for efficiency and internal conversion. Energies and intensities of transitions not placed in the level scheme are shown below the main table.

| Level energy (keV)            | $J^\pi$  | Transition energy (keV) | Relative intensity | Multipolarity |
|-------------------------------|----------|-------------------------|--------------------|---------------|
| 432.6(2)                      | $2^+$    | 432.6(2)                | 100                | $E2$          |
| 936.3(3)                      | $4^+$    | 503.7(2)                | 80(8)              | $E2$          |
| 1500.6(3)                     | $6^+$    | 564.3(2)                | 35(3)              | $E2$          |
| 1776.3(4)                     | $6^+$    | 840.0(2)                | 30(5)              | $E2$          |
| 2033.6(4)                     | $8^+$    | 257.3(2)                | 28(4)              | $E2$          |
| 2114.0(4)                     | $8^+$    | 613.4(2)                | 19(4)              | $E2$          |
| 2300.5(4)                     | $9^-$    | 266.9(2)                | 14(4)              | $E1/M2$       |
| 2554.1(5)                     | $(10^+)$ | 440.1(3)                | 22(2)              |               |
| 2776.2(6)                     | $(12^+)$ | 222.1(3)                | 5(2)               |               |
| Unplaced transitions:         |          |                         |                    |               |
|                               |          | 429.1(3)                | 10(2)              |               |
|                               |          | 482.6(3)                | 12(2)              |               |
|                               |          | 492.1(3)                | 14(2)              |               |
| Unplaced delayed transitions: |          |                         |                    |               |
|                               |          | 160.9(3)                |                    |               |
|                               |          | 182.8(6)                |                    |               |

transitions have distributions which rise with  $\cos^2\theta$ . This indicates that they are consistent with assignments of stretched quadrupole transitions. The 267-keV transition is different in that it has a downsloping distribution indicative of a stretched dipolar multipolarity. These assignments are in general agreement with the systematics of the radon isotopes as discussed in detail below, which also suggest an  $E1$  nature for the 267-keV transition.

Figure 4 shows a spectrum of delayed  $\gamma$ -ray energies observed at the focal plane of RITU which are correlated with recoil- $\alpha$  decay sequences identified with  $^{200}\text{Rn}$ . This spectrum is the sum of data taken in both  $^{200}\text{Rn}$  experiments, with and without the target array in place. The  $4^+ \rightarrow 2^+$  and  $2^+ \rightarrow 0^+$  transitions are clearly seen with energies of 433 and 504 keV, along with the  $6_2^+ \rightarrow 4^+$  transition, with an energy of 840 keV, and transitions above it. No transitions are observed from the pathway involving the yrast  $6^+$  state, confirming the existence of the two parallel pathways in the proposed level scheme. Two low-energy transitions with energies 161 and 183 keV are also observed which deexcite the isomer and feed the states above the  $6_2^+$  state. The exact details of this feeding remain tentative as coincidence data at the focal plane is not possible given the weakness of the isomer population. However, on the assumption that the 257- and 267-keV transitions have the same detection efficiency, the ratio of their intensities in the focal plane spectrum is 1.5(4), which suggests that the isomer decay feeds into the  $8_1^+$  state as well as the  $9^-$  state.

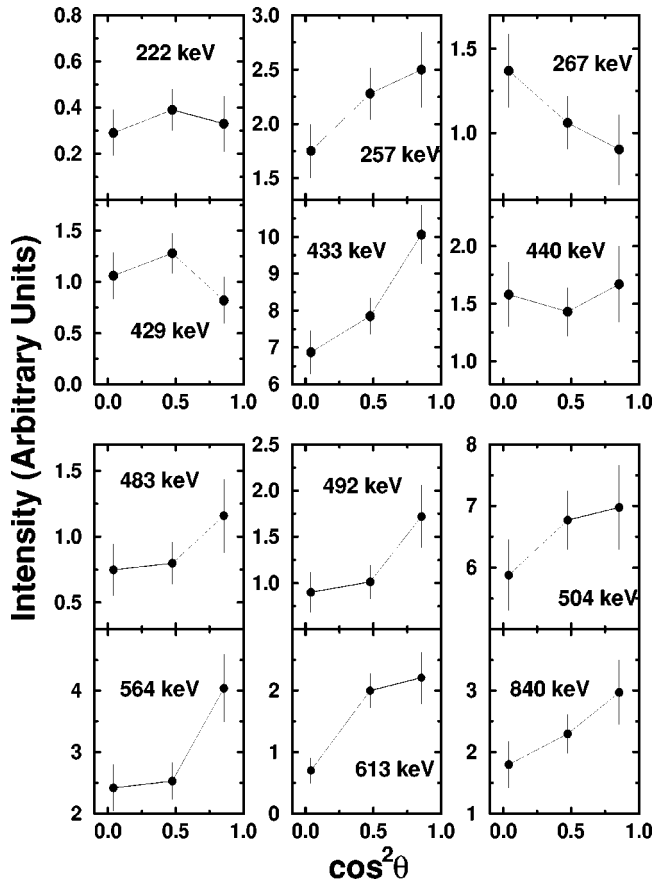


FIG. 3. Angular distributions of  $\gamma$  rays measured in the decay of excited states of  $^{200}\text{Rn}$  plotted as a function of  $\cos^2\theta$ . The data shown are derived from singles  $\gamma$ -ray events correlated with  $^{200}\text{Rn}$   $\alpha$  decays.

Measured time intervals between implantation and  $\gamma$  decay in events which are correlated with  $\alpha$  decays of  $^{200}\text{Rn}$ , shown in Fig. 5, yield a value of  $36_{-8}^{+16}$   $\mu\text{s}$  for the mean life of the isomer. Figure 6 shows a spectrum of prompt  $\gamma$  rays which are in coincidence with a recoiling ion which subsequently emitted delayed  $\gamma$  rays at the focal plane with energies corresponding to transitions in  $^{200}\text{Rn}$ , both with and without the condition that the recoiling ion also  $\alpha$  decays with the energy corresponding to  $^{200}\text{Rn}$ . These spectra give evidence of a prompt  $\gamma$ -ray transition with an energy of 482.4(3) keV which feeds the isomer. This is consistent with a transition seen in the decay-correlated prompt  $\gamma$ -ray energy spectrum (see Fig. 2), which has a transition of energy 482.6(3) keV.

### B. Level scheme of $^{202}\text{Rn}$

The previous published work on  $^{202}\text{Rn}$  is restricted to the knowledge of the first few excited states, up to the yrast spin-8 state, from recoil- $\gamma$  measurements [16]. The association of these transitions with  $^{202}\text{Rn}$  was confirmed by radioactive-decay correlation techniques [17], but in both cases the construction of the level scheme relied on intensities and comparison with systematics. The current work uses a recoil separator with higher transmission than that used in

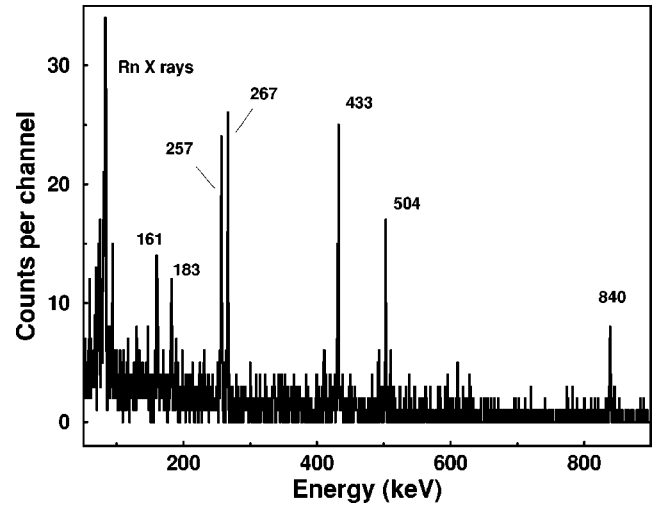


FIG. 4. Energy spectrum of delayed  $\gamma$  rays emitted at the focal plane by ions which subsequently  $\alpha$  decay at the focal plane with characteristics which are associated with  $^{200}\text{Rn}$ . Strong peaks are labeled by the transition energy in keV.

Refs. [16,17], which has allowed the level scheme to be confirmed and extended using recoil- $\gamma$ - $\gamma$  techniques. Angular distribution measurements have also confirmed some of the spin assignments, which were all previously based on systematics.

Analysis of  $\alpha$ -particle energy spectra at the focal plane indicates that  $^{202}\text{Rn}$  is the dominant evaporation residue from the reaction of  $^{40}\text{Ar}$  on  $^{166}\text{Er}$ ; other isotopes, particularly  $^{201,203}\text{Rn}$ , are only present with yields of less than 15% of the main channel. The production cross section is estimated to be 300  $\mu\text{b}$  from the  $\alpha$ -particle yield using assumptions similar to those made for  $^{200}\text{Rn}$  above. The half-life of  $^{202}\text{Rn}$  is 9.9(2) s, which begins to be comparable to the av-

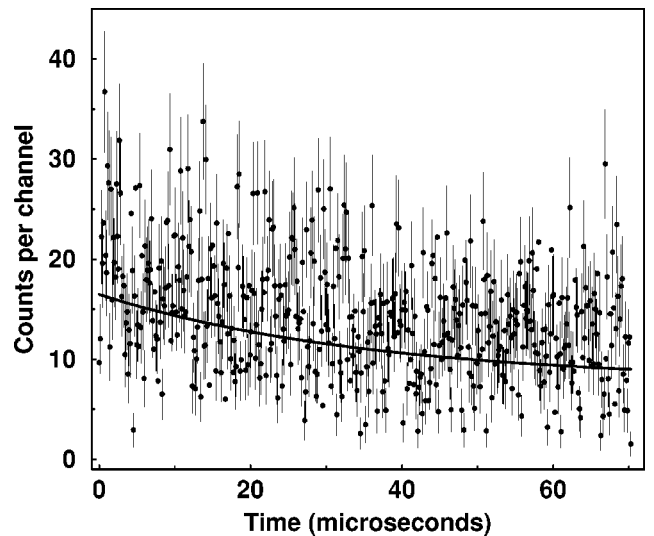


FIG. 5. Time intervals between implantation and focal-plane  $\gamma$  decay. Events here are correlated with subsequent  $\alpha$  decays characteristic of  $^{200}\text{Rn}$ . The solid line represents a least-squares fit to the data of the form  $y = a + be^{-t/\tau}$ . The inferred mean lifetime is  $36_{-8}^{+16}$   $\mu\text{s}$ .

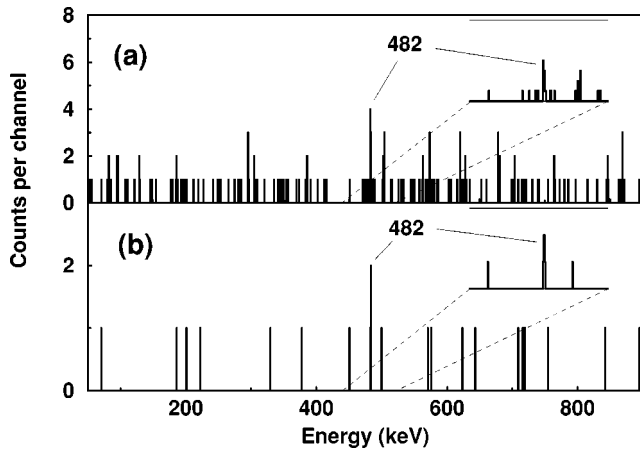


FIG. 6. Energy spectra of prompt  $\gamma$  rays which are in coincidence with recoiling ions which subsequently emit  $\gamma$  rays at the focal plane with energies corresponding to those associated with the isomeric decay observed in  $^{200}\text{Rn}$  (see Fig. 4). The events shown in (b) have the additional requirement that the recoil  $\alpha$  decays with characteristics associated with  $^{200}\text{Rn}$ . The insets show expanded portions of the spectrum in order to give an impression of the width of candidate peaks, with the same vertical range as the main spectrum. Peaks are labeled by the transition energy to the nearest keV.

erage time interval between events at a particular position in the silicon detector. Since the low-lying transitions have already been associated with  $^{202}\text{Rn}$  decays, recoil- $\alpha$  correlations were not performed. Recoil- $\gamma$ - $\gamma$  data were used to construct the level scheme on the basis of coincidences between transitions, intensities in gated spectra and energy-sum arguments. The resulting scheme is shown in Fig. 7. The level scheme shows two pathways in the low-lying states, similar to those observed in  $^{200}\text{Rn}$ , which can be justified with reference to gates placed on the 504-, 569-, 625-, and 717-keV transitions shown in Fig. 8. Energies and intensities of  $\gamma$  rays can be found in Table II. Of particular interest is the weak side structure which feeds into the first excited state. A spectrum gated on the 526-keV transition [see Fig. 9(a)] clearly shows coincidence with the 504-keV transition, but no other

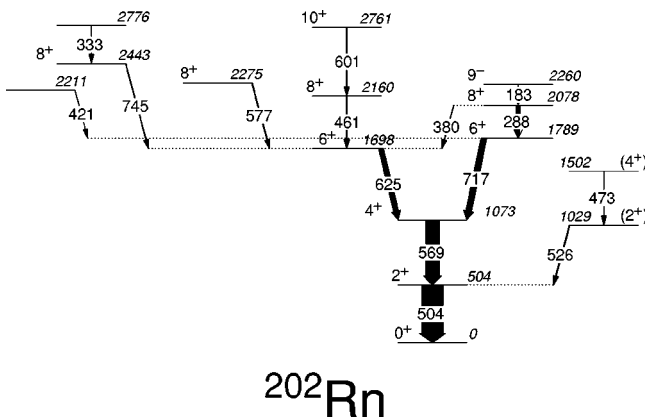


FIG. 7. The level scheme for  $^{202}\text{Rn}$  deduced from measurements of the  $^{166}\text{Er}(^{40}\text{Ar},n)$  reaction. Transitions are labeled with the transition energy to the nearest keV. Excited states are labeled by the assigned spin-parity and excitation energy in keV.

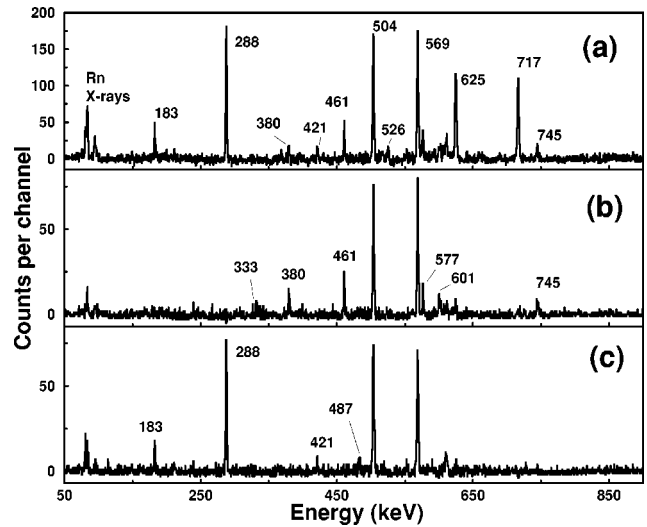


FIG. 8. Gated  $\gamma$ -ray energy spectra associated with  $^{202}\text{Rn}$ : (a) a sum of spectra gated on energies of 504 and 569 keV, (b) a spectrum gated on an energy of 625 keV, and (c) a spectrum gated on an energy of 717 keV. Transitions of interest are labeled by the transition energy to the nearest keV. Background subtraction was performed using the method of Ref. [24].

low-lying  $\gamma$  rays, along with a transition at 473 keV. This justifies the feeding of a weak side structure into the first excited state.

In a similar fashion to the  $^{200}\text{Rn}$  analysis, the data were used to generate three-point angular distributions of  $\gamma$ -ray intensity which were used to assist spin assignments. The results are shown in Fig. 10, where distributions which slope upwards are assigned as stretched quadrupole transitions, and down sloping distributions, such as that for the 183-keV transition, are assigned to be dipolar in nature. There were insufficient statistics in gated spectra to tie down the nature of the 183-keV transition on the basis of conversion coefficient arguments; it is assumed here to be an electric dipole transition on the basis of the similarity in the decay pattern with  $^{204}\text{Rn}$  discussed in the next section. The states in the weak side structure at energies of 1030 and 1502 keV are tentatively assigned to be  $2^+$  and  $4^+$ , respectively. The only other reasonable possibility would be spins of 4 and  $6\hbar$ , but this would make these states yrast with the expectation that they would be associated with much stronger feeding. It is also noted that the angular distribution of the 526-keV transition is not clearly of either stretched quadrupole or stretched dipole character, and may be indicative of a  $\Delta J = 0$  transition. Given the possible interpretations of this side structure, it is of interest to investigate possible  $E0$  components in the decay. A gate was placed on the 473-keV transition in order to assess the relative radiative intensity in the 526-keV transition. Figure 9(b) shows the raw gate on an energy of 473 keV without removing any background to illustrate the importance of the subtraction technique. The 526-keV transition is clearly visible, along with other lines arising due to background contributions. In order to remove them, a fraction of the total projection was subtracted and the result is shown in Fig. 9(c). Most of the low-lying transitions arising from the background have disappeared, but some in-

TABLE II. Energies and deduced spins of excited states in  $^{202}\text{Rn}$ . Measured transition energies and relative intensities of prompt deexciting  $\gamma$  rays are listed along with the inferred multiplicities. Relative intensities of transitions are listed and have been corrected for efficiency and internal conversion. Energies and intensities of transitions not placed in the level scheme are shown below the main table. Intensities are taken from fitting the  $\gamma$ - $\gamma$  matrix, except those marked by an asterisk which are taken from the total projection.

| Level energy (keV)            | $J^\pi$ | Transition energy (keV) | Relative intensity | Multipolarity |
|-------------------------------|---------|-------------------------|--------------------|---------------|
| 504.0(1)                      | $2^+$   | 504.0(1)                | 100*               | $E2$          |
| 1029.7(3)                     | $(2^+)$ | 525.7(3)                | 5(1)               | $\Delta J=0$  |
| 1073.1(2)                     | $4^+$   | 569.1(2)                | 88(4)              | $E2$          |
| 1502.2(6)                     | $(4^+)$ | 472.5(5)                | 1.2(6)             |               |
| 1698.3(3)                     | $6^+$   | 625.2(2)                | 32(2)              | $E2$          |
| 1789.4(4)                     | $6^+$   | 716.7(3)                | 38(2)              | $E2$          |
| 2077.9(3)                     | $8^+$   | 287.8(2)                | 24(1)              | $E2$          |
|                               |         | 379.9(3)                | 2.3(4)             | $(E2)$        |
| 2159.6(4)                     | $8^+$   | 461.3(3)                | 5.8(7)             | $E2$          |
| 2210.9(5)                     |         | 421.1(2)                | 1.4(5)             |               |
| 2260.4(4)                     | $9^-$   | 182.5(3)                | 3.3(4)             | $E1/M2$       |
| 2275.1(4)                     | $8^+$   | 576.8(3)                | 4.9(7)             | $E2$          |
| 2443.0(5)                     | $8^+$   | 744.7(4)                | 3.7(7)             | $E2$          |
| 2760.6(6)                     | $10^+$  | 601.0(4)                | 3.4(5)             | $E2$          |
| 2775.7(8)                     |         | 332.6(6)                | 0.3(3)             |               |
| Unplaced prompt transitions:  |         | 486.9(5)                | 11.1(5)*           |               |
| Unplaced delayed transitions: |         | 110.9(4)                |                    |               |
|                               |         | 148.8(4)                |                    |               |
|                               |         | 211.5(3)                |                    |               |

tensity remains in the 504-keV peak, indicating real coincidence with the 473-keV transition as expected from the level scheme presented. In Fig. 9(c) the intensity of the two lines are the same to within errors; the percentage missing intensity in the 526-keV transition is measured to be  $-54(71)\%$ . The current data clearly do not have the statistical precision with which to address the issue of  $E0$  components. Systematic effects in the background subtraction technique will also be important. Such issues also prohibitively effect other methods of shedding light on the issue, such as the measurement of x-ray yields associated with different decay paths in the level scheme. The question of the size of any  $E0$  component in the 526-keV transition is therefore open. It is noted that similar problems have arisen in assessing  $E0$  strength contributions in Po isotopes; statistically consistent measurements have been used to draw different conclusions about the same transition [7,8] (see Ref. [9] for further discussion).

Inspection of  $\gamma$ -ray emissions at the focal plane indicates the presence of an isomer with a lifetime longer than the flight time through RITU. Figure 11(a) shows a spectrum of  $\gamma$  rays within a time period of up to  $30 \mu\text{s}$  after the implan-

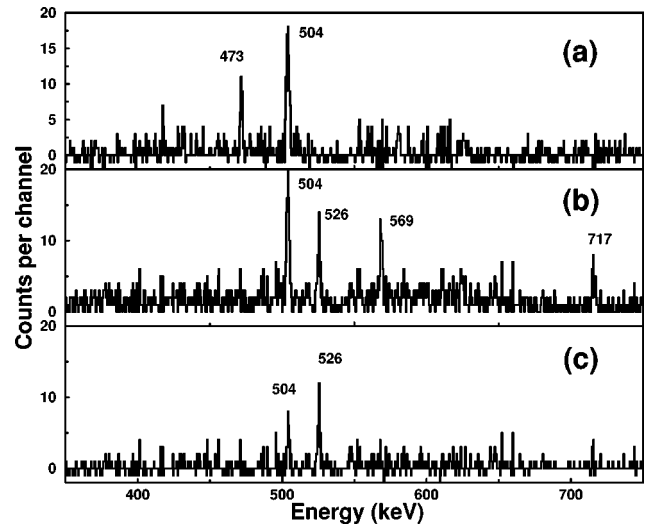


FIG. 9. Gated  $\gamma$ -ray energy spectra associated with the weak low-lying sideband structure in  $^{202}\text{Rn}$ : (a) a gate on an energy of 526 keV, (b) a gate on an energy of 473 keV without background subtraction, and (c) a gate on an energy of 473 keV with a fraction of the total projection spectrum subtracted.

tation of a recoil. Transitions are clearly present which belong to one of the two branches of the near-yrast level scheme of  $^{202}\text{Rn}$  (see Fig. 7), namely, the branch associated with the yrast  $9^-$  state. Gates were placed on the energies of

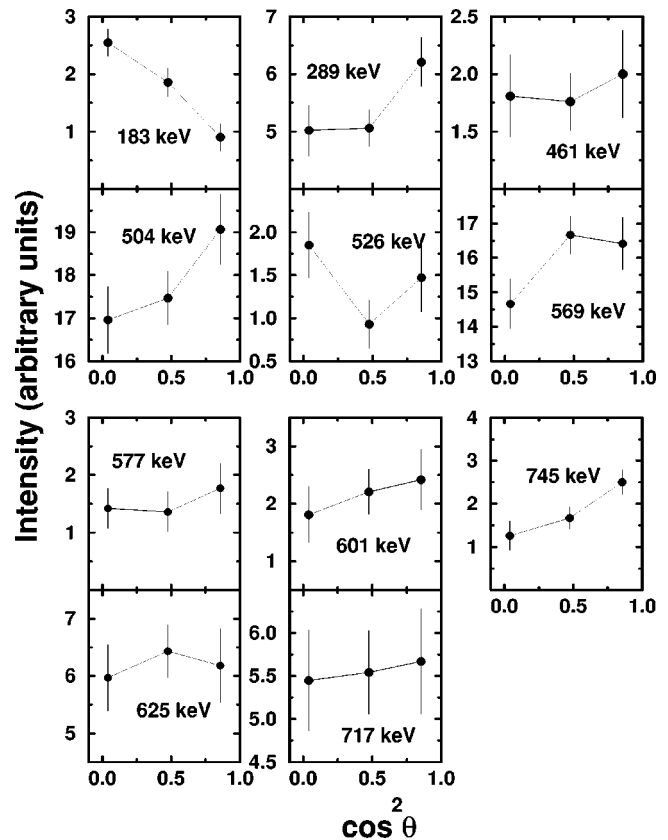


FIG. 10. Angular distributions of  $\gamma$  rays measured in the decay of excited states of  $^{202}\text{Rn}$  plotted as a function of  $\cos^2\theta$ .

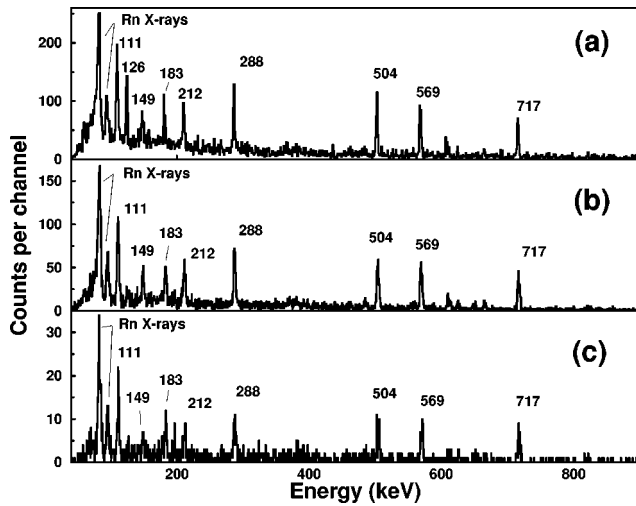


FIG. 11. Energy spectra of  $\gamma$  rays emitted at the focal plane in the  $^{202}\text{Rn}$  experiment under various conditions: (a) events within a time period of up to  $\sim 30 \mu\text{s}$  following the implantation of a recoiling ion in to the silicon detector, (b) events within a time period of  $\sim 4.6 \mu\text{s}$  following implantation, and (c)  $\gamma$ - $\gamma$  events at the focal plane in the time period of  $\sim 30 \mu\text{s}$  after recoil implantation.

known transitions associated with  $^{202}\text{Rn}$  (see Table II) and the resulting time intervals between implantation and focal-plane  $\gamma$ -ray emission were analyzed to yield a mean life of  $3.2(1) \mu\text{s}$  for this isomer, as shown in Fig. 12.

Placing time gates on the focal plane  $\gamma$ -ray data, indicates that not all of the transitions indicated in Fig. 11(a) are from the decay of this isomer; Fig. 11(b) shows the same spectrum but gated with a time window restricting  $\gamma$ -ray emission to  $4.6 \mu\text{s}$  after the arrival of a recoil. Notice in particular that a transition with an energy of  $125.9(4) \text{ keV}$  is no longer present in this spectrum, suggesting that it is associated with a much longer isomeric decay. This transition is also absent in a focal-plane  $\gamma$ - $\gamma$  total projection spectrum [see Fig.

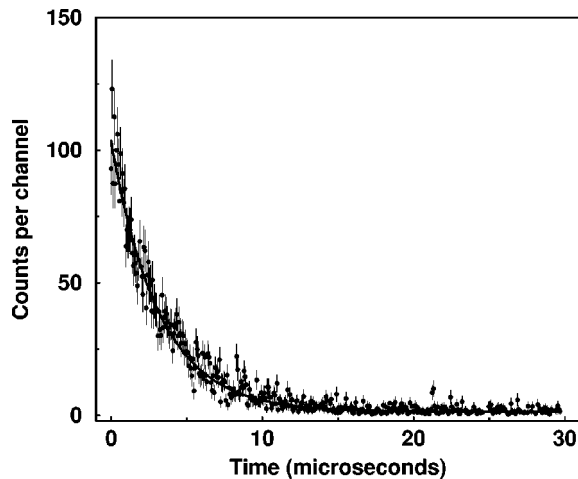


FIG. 12. The distribution of time intervals between implantation and focal-plane  $\gamma$ -ray emission for events involving  $\gamma$ -ray transitions associated with  $^{202}\text{Rn}$ . The solid line represents a least-squares fit to the data of the form  $y = a + be^{-t/\tau}$ . The inferred mean lifetime is  $3.2(1) \mu\text{s}$ .

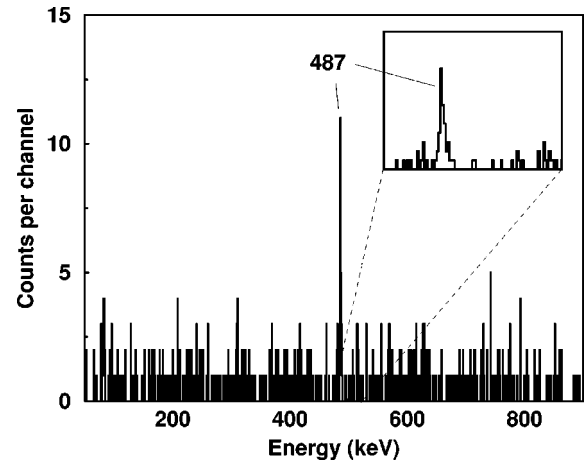


FIG. 13. Energy spectra of prompt  $\gamma$  rays which are in coincidence with recoiling ions which subsequently emit  $\gamma$  rays at the focal plane with energies corresponding to those associated with the isomeric decay observed in  $^{202}\text{Rn}$ . The inset shows an expanded portion of the spectrum with the same vertical range as the main spectrum, in order to illustrate the width of the peak in the spectrum.

11(c)], indicating that it is not associated with a decay path with a large  $\gamma$ -ray multiplicity. It is likely that this longer-lived isomer is associated with one of the more weakly produced reaction channels such as  $^{201,203}\text{Rn}$ . The  $\gamma$ - $\gamma$  data was insufficient to allow detailed information on the decay path of the isomer to be established. Consideration of the balance of  $\gamma$ -ray flux through states populated in the decay of the isomer suggests that the decay feeds the  $8_1^+$  state at  $2078 \text{ keV}$  excitation at a level of  $56(10)\%$  and the  $9^-$  state at  $2260 \text{ keV}$  at a level of  $35(7)\%$ . Unlike the case of  $^{200}\text{Rn}$  where the two transitions are of similar energy, these numbers are subject to a systematic error involving the relative efficiencies of the 183- and 288-keV transitions; the relative efficiency measurement is performed using a point source, whereas the implanted ions are spread over the area of the implantation detector.

In order to establish candidates for transitions which feed the isomer in  $^{202}\text{Rn}$ , a spectrum was produced of prompt  $\gamma$  rays emitted from recoiling ions which, after implantation at the focal plane, produce delayed  $\gamma$  rays with energies corresponding to transitions assigned to  $^{202}\text{Rn}$ . The results are shown in Fig. 13 which clearly shows a transition with an energy of  $486.8(2) \text{ keV}$ . This transition is present in the total projection of prompt  $\gamma$ - $\gamma$  events with energy of  $486.9(5) \text{ keV}$ .

### C. Level scheme of $^{204}\text{Rn}$

There are two previously published papers on  $^{204}\text{Rn}$ . The first [25] consisted of  $\gamma$ - $\gamma$  measurements made with a small number of detectors with no channel selection; isotopic assignments were made on the basis of excitation functions. A level scheme with 28 transitions was produced but the current findings are only consistent with a subset of these, the others presumably arose from contaminants in competing reaction channels. A recoil- $\gamma$  measurement with mass selection

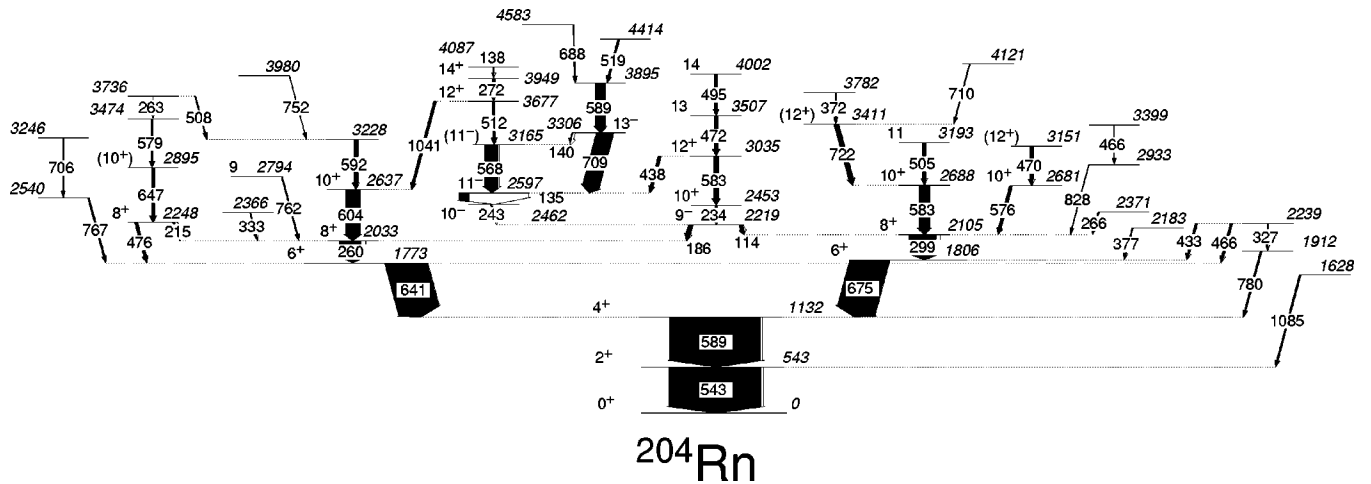


FIG. 14. The decay scheme of  $^{204}\text{Rn}$  deduced from recoil-gated  $\gamma$ - $\gamma$  measurements in the  $^{168}\text{Er}(^{40}\text{Ar},4n)$  reaction at a beam energy of 177 MeV. Transitions are labeled with the transition energy given to the nearest keV. Excited states are labeled by the spin parity, assigned using measured DCO ratios as detailed in the text, and, in italics, by the excitation energy in keV.

has also been performed [16] where the low-lying transitions up to the yrast  $J^\pi = 9^-$  state were confirmed, but the use of a low efficiency array of  $\gamma$ -ray detectors prevented any coincidence work.

In the  $^{40}\text{Ar} + ^{168}\text{Er}$  reaction,  $^{204}\text{Rn}$  is the dominant channel with the only other significant residues being the neighboring odd isotopes present at a similar level to the  $^{202}\text{Rn}$  experiment. The current analysis is based on recoil-selected  $\gamma$ - $\gamma$  measurements, which has established the level scheme shown in Fig. 14, involving a total of 54 transitions, 36 of which have not been previously reported. The yrast levels up to spin  $13\hbar$  are consistent with the work of Ref. [25]. There is a notable loss of intensity between the 135- and 243-keV transitions feeding into and out of a state assigned to be  $10^-$  at 2460 keV excitation. This state is isomeric with a previously measured lifetime of 33(3) nsec [25]; analysis of the time spectrum associated with the 243-keV transition yields a consistent measurement of the lifetime of 34(4) ns (see Ref. [26] for details). The addition of a large number of weak transitions from a variety of nonyrast states to the yrast level scheme and the introduction of two pairs of transitions with similar energies (a 589.2 keV transition with an energy similar to the  $4^+ \rightarrow 2^+$  588.6-keV transition and two transitions with energies of 582.6 and 583.0 keV) have lead to extension and significant revision of the previous level scheme. Energies and intensities of  $\gamma$  rays can be found in Table III.

Evidence for a second 589-keV transition is clear from a spectrum gated on a transition with an energy of 135 keV, shown in Fig. 15(a). This transition is above the 34 ns isomer discussed above, so the transitions below show a reduced intensity compared to those above. For example the 543-keV transition is weak compared to the 709-keV transition. However, there is a strong 589-keV transition in this gate which indicates a transition of similar energy to the  $4^+ \rightarrow 2^+$  transition above the isomer. Closer inspection of the centroids of such peaks in gates above and below the isomer, yields 588.6(1) keV for the transition below, and 589.2(3) keV for the transition above the isomer. Figure 15(b) and (c) show spectra gated on the 299-keV transition and a sum of 234-

keV and 114-keV transitions respectively. Peaks corresponding to a  $\gamma$ -ray energy of around 583 keV are present in both gates, however, a consistent picture can only be found if these peaks arise from different transitions and in fact the extracted transition energies are different from one another (see Table III). There is a broad peak in the 299 keV gate around 185 keV [see Fig. 15(b)]. This does not arise from  $^{204}\text{Rn}$ , but from Coulomb excitation which presumably appears in the data due to a weak scattered beam group reaching the focal plane of RITU. The yrast  $6^+ \rightarrow 4^+$  transition in  $^{168}\text{Er}$  has an energy of 285 keV which contaminates the 299-keV gate as it is broadened due to kinematic effects. The  $2^+ \rightarrow 0^+$  transition has an energy of 80 keV which also appears in the spectrum unresolved from the Rn x-ray group. An interesting example of a weak nonyrast transition is that which feeds directly into the  $2_1^+$  level with a transition energy of 1085 keV. A gate on that transition [see Fig. 15(d)] yields a very clean and empty spectrum, other than a peak corresponding to the  $2^+ \rightarrow 0^+$  transition at 543 keV.

Given the complexity of the deduced level scheme, simple angular distribution measurements were not performed and a  $\gamma$ - $\gamma$  directional correlation technique was used to provide the necessary spectrum cleanliness. The germanium detectors were grouped into two sets; central-angle detectors at  $79^\circ$  and  $101^\circ$  and backward-angle detectors at  $134^\circ$  and  $158^\circ$  to the beam axis. Data were sorted into a central-versus backward-angle two-dimensional matrix and an experimental DCO ratio for each transition was defined as

$$R_{\text{DCO}} = I_{\text{back}}^{\gamma_2}(\text{gate}_{\text{cent}}^{\gamma_1}) / I_{\text{cent}}^{\gamma_2}(\text{gate}_{\text{back}}^{\gamma_1}),$$

where  $I_a^{\gamma_i}(\text{gate}_b^{\gamma_j})$  is the intensity of  $\gamma_i$  measured in detector group  $a$  in a spectrum gated by  $\gamma_j$  measured in detector group  $b$ . The results are listed in Table III. The empirical results for transitions with known multipolarity are consistent with schematic calculations using the formalism in Ref. [27], although full calculations involving an efficiency weighted average over all detector pairs have not been per-

TABLE III. Energies and deduced spins of excited states in  $^{204}\text{Rn}$ . Measured transition energies, relative intensities, and DCO ratios for deexciting  $\gamma$ -ray transitions are listed along with the assigned multipolarity and spin change. DCO ratios are defined in detail in the text; the gating transition is a stretched quadrupole transition unless marked by an asterisk where stretched dipole transitions have been used.

| Level energy |            |            |            |                  | M        |            | Level energy |            |            |            |                  | M        |            |
|--------------|------------|------------|------------|------------------|----------|------------|--------------|------------|------------|------------|------------------|----------|------------|
| (keV)        | $J^\pi$    | $E_\gamma$ | $I_\gamma$ | $R_{\text{DCO}}$ | (L)      | $\Delta J$ | (keV)        | $J^\pi$    | $E_\gamma$ | $I_\gamma$ | $R_{\text{DCO}}$ | (L)      | $\Delta J$ |
| 542.9(1)     | $2^+$      | 542.9(1)   | 100        | 0.99(2)          | $E2$     | 2          | 2933.0(2)    | ( $10^+$ ) | 828.0(1)   | 0.7(1)     |                  |          |            |
| 1131.5(1)    | $4^+$      | 588.6(1)   | 99(4)      | 1.04(4)          | $E2$     | 2          | 3035.1(3)    | $12^+$     | 438.0(4)   | 3.3(3)     | 1.0(2)*          | $E1$     | 1          |
| 1627.8(1)    | (2-4)      | 1084.9(13) | 1.8(4)     |                  |          |            |              |            | 582.6(2)   | 5.6(3)     | 1.3(2)           | $E2$     | 2          |
| 1772.8(2)    | $6^+$      | 641.3(1)   | 45(2)      | 0.98(4)          | $E2$     | 2          | 3150.9(3)    | ( $12^+$ ) | 469.9(2)   | 3.8(2)     | 1.0(2)           | ( $E2$ ) | (2)        |
| 1806.2(2)    | $6^+$      | 674.7(1)   | 42(2)      | 0.99(3)          | $E2$     | 2          | 3165.1(5)    | ( $11^-$ ) | 568.3(3)   | 14(1)      | 0.8(1)*          | ( $M1$ ) | 1          |
| 1911.4(6)    | (4,5)      | 779.9(6)   | 1.8(4)     |                  |          |            | 3192.9(4)    | 11         | 504.9(3)   | 3.0(2)     | 0.6(1)           |          | 1          |
| 2032.7(2)    | $8^+$      | 259.9(1)   | 23(1)      | 0.97(4)          | $E2$     | 2          | 3228.5(5)    | (11,12)    | 591.9(3)   | 4.1(2)     |                  |          |            |
| 2105.0(2)    | $8^+$      | 298.9(1)   | 30(1)      | 0.95(4)          | $E2$     | 2          | 3246(1)      | ( $10^+$ ) | 706.4(10)  | 0.6(1)     |                  |          |            |
| 2182.7(5)    | (6,7)      | 376.5(5)   | 1.3(2)     |                  |          |            | 3305.4(3)    | $13^-$     | 140.3(4)   | 1.3(1)     |                  |          |            |
| 2218.8(2)    | $9^-$      | 113.7(1)   | 3.8(2)     | 0.81(7)          | $E1$     | 1          |              |            | 708.6(2)   | 18.2(1)    | 1.6(2)*          | $E2$     | 2          |
|              |            | 186.1(1)   | 4.7(2)     | 0.88(6)          | $E1$     | 1          | 3399(1)      | (11,12)    | 465.6(10)  | 0.4(1)     |                  |          |            |
| 2239.1(3)    | (7)        | 327.0(5)   | 1.0(1)     |                  |          |            | 3410.4(3)    | ( $12^+$ ) | 722.4(2)   | 5.1(3)     | 1.7(3)           | ( $E2$ ) | (2)        |
|              |            | 433.2(4)   | 2.4(2)     |                  |          |            | 3473.7(5)    | (11,12)    | 578.7(3)   | 2.1(2)     |                  |          |            |
|              |            | 466.4(4)   | 2.5(2)     |                  |          |            | 3506.9(4)    | 13         | 471.8(2)   | 4.8(3)     | 1.0(1)*          | $E1$     | 1          |
| 2248.2(2)    | $8^+$      | 215.3(2)   | 2.0(1)     | 1.1(2)           | $M1$     | 0          | 3677.0(4)    | $12^+$     | 511.6(3)   | 2.7(2)     | 0.7(1)           | $E1$     | 1          |
|              |            | 475.6(3)   | 3.1(2)     | 0.9(2)           | $E2$     | 2          |              |            | 1040.6(3)  | 2.7(2)     | 1.0(2)           | $E2$     | 2          |
| 2365.5(4)    | (8,9)      | 332.8(4)   | 1.0(1)     |                  |          |            | 3736.5(6)    | (12-14)    | 262.9(8)   | 0.33(6)    |                  |          |            |
| 2371.1(3)    | (8,9)      | 266.1(3)   | 1.4(1)     |                  |          |            |              |            | 508.0(4)   | 1.3(1)     |                  |          |            |
| 2452.8(3)    | $10^+$     | 234.0(2)   | 2.2(1)     | 0.78(10)         | $E1$     | 1          | 3782.2(5)    | (12-14)    | 371.8(4)   | 1.0(9)     |                  |          |            |
| 2461.4(4)    | $10^-$     | 242.8(4)   | 0.87(9)    | 0.8(2)           | $M1$     | 1          | 3894.6(5)    | (13-15)    | 589.2(3)   | 10.5(7)    |                  |          |            |
| 2540.0(6)    | ( $8^+$ )  | 767.2(6)   | 1.8(2)     |                  |          |            | 3948.8(4)    | $14^+$     | 271.8(2)   | 2.8(2)     | 1.0(3)           | $E2$     | 2          |
| 2596.8(4)    | $11^-$     | 135.2(2)   | 11.1(4)    | 0.9(2)*          | $M1$     | 1          | 3980(1)      | (12-14)    | 751.7(12)  | 0.5(1)     |                  |          |            |
| 2636.6(4)    | $10^+$     | 603.9(1)   | 15.5(8)    | 1.03(5)          | $E2$     | 2          | 4001.7(4)    | 14         | 494.8(2)   | 2.9(2)     | 0.9(1)*          | $E1$     | 1          |
| 2681.0(3)    | $10^+$     | 576.0(2)   | 3.2(2)     | 1.1(2)           | $E2$     | 2          | 4087.2(5)    | (14-16)    | 138.4(3)   | 0.9(1)     |                  |          |            |
| 2688.0(3)    | $10^+$     | 583.0(2)   | 11.7(5)    | 1.2(1)           | $E2$     | 2          | 4120.6(8)    | (13,14)    | 710.2(7)   | 0.9(1)     |                  |          |            |
| 2794.3(4)    | 9          | 761.6(6)   | 1.3(2)     | 0.8(1)           | $M1$     | 1          | 4413.5(5)    | (14-17)    | 518.9(5)   | 2.2(2)     |                  |          |            |
| 2895.0(4)    | ( $10^+$ ) | 646.8(3)   | 3.8(2)     | 0.8(2)           | ( $E2$ ) | (2)        | 4582.8(9)    | (14-17)    | 688.2(8)   | 1.3(2)     |                  |          |            |

formed. The ratio for a stretched quadrupole transition gated by another stretched quadrupole transition should be equal to unity, which is the case for the known low-lying quadrupole transitions, for example, the 543- and 589-keV transitions have  $R_{\text{DCO}}$  ratios of 0.99(2) and 1.04(4) when gated on each other. The 186-keV transition has previously been assigned to have a dipolar nature on the basis of an angular distribution measurement [25]. When gated by a stretched quadrupole transition, the ratio obtained for the 186-keV transition is 0.77(6). This is consistent with the result of a schematic calculation (0.68) with detectors at  $90^\circ$  and  $142^\circ$  and a typical alignment parameter of  $\sigma/J=0.4$  for a primary state of similar spin. These internally calibrated ratios were then used to assign the spin changes involved in the other transitions observed. (Note that some transitions, marked by an asterisk in Table III, are gated by dipolar transitions in order to obtain clean gated spectra.)

Spin assignments in the level scheme have been made primarily on the basis of measured DCO ratios. Where transitions involve a substantial contribution from internal conversion, intensity arguments have been used to back up the assigned spin and to infer the multipolarity involved. In the

absence of these measurements, through lack of adequate statistics or spectrum cleanliness, tentative assignments are made on the basis of yrast or near-yrast feeding arguments assuming that stretched transitions are prevalent. For clarity, assignments made solely on the basis of feeding arguments are not shown on the level scheme Fig. 14, but are listed in Table III.

The strong low-lying transitions all have DCO ratios consistent with stretched quadrupole transitions, giving spin-parity assignments for the two main deexcitation pathways up to  $J^\pi=8^+$ . The 186- and 114-keV transitions have DCO ratios which are less than one. If they are assigned to be  $E1$  transitions, a consistent picture of the intensities in a spectrum gated on an energy of 234 keV arises after conversion correction. Assignments of  $E1$  and  $M1$  multipolarity are made to the 234- and 135-keV transitions on a similar basis.

Several parallel branches in the level scheme assist multipolarity assignments. The parallel pair of transitions with energies 476 and 215 keV feed the yrast  $6^+$  and  $8^+$  states respectively from a level at an excitation energy of 2248 keV. The DCO ratio for the former is consistent with a stretched quadrupole transition, whilst intensities of the transitions are

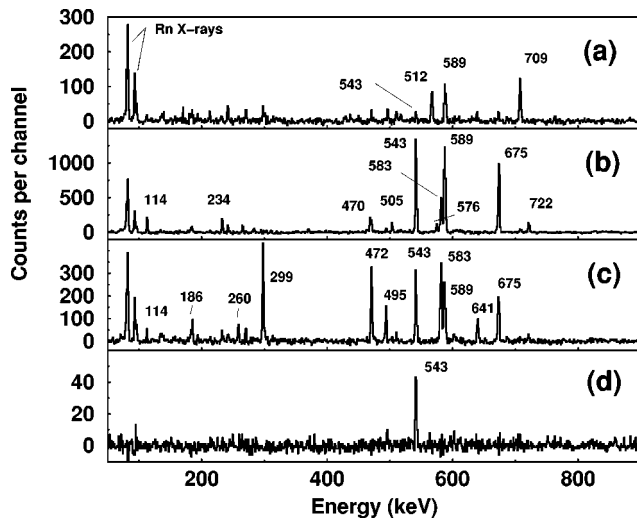


FIG. 15. Energy spectra of prompt  $\gamma$  rays emitted at the target position in the  $^{204}\text{Rn}$  experiment: (a) gated by a transition energy of 135 keV, (b) gated by a transition energy of 299 keV, (c) gated by a transition energy of 114 or 234 keV, and (d) gated by a transition energy of 1085 keV. The prominent peaks in the spectrum are labeled with the transition energy given to the nearest keV.

consistent with a magnetic dipole conversion coefficient for the 215-keV transition. Its measured DCO ratio is 1.1(2) which is not inconsistent with the schematic calculation for a  $\Delta J=0$  transition, which yields 1.04 under the assumptions stated above. This leads to a  $J^\pi=8^+$  assignment for the de-exciting state. The parallel pair of transitions with energies of 568 and 709 keV were observed by Ref. [25] but the 140-keV crossover was not. The 1041- and 512-keV transitions have DCO ratios consistent with stretched quadrupole and dipole nature, respectively, so it is likely that the 568-keV transition deexcites a spin-11 state. This would require that the 140-keV transition have quadrupole multipolarity; consistent intensities are obtained for an  $E2$  rather than an  $M2$  transition, fixing the spin-parity to be  $11^-$ . The 438-keV transition feeds into this state and has a DCO ratio of 0.97(16) when gated by a dipolar transition. This suggests a  $12^+$  assignment for the deexciting state. Measured DCO ratios in the parallel path via 583- and 234-keV transitions to the yrast  $9^-$  state are consistent with this. The authors of Ref. [25] note that the temporal character of these two transitions suggests that they are partially fed by a delayed component with a half-life around 10 ns. The time spectra associated with the 234-, 438-, and 583-keV transitions are all consistent with some delayed feeding component; analysis of the time spectra for the 234- and 438-keV transitions gives a half-life of 14(4) ns [26] consistent with Ref. [25]. The 495- and 472-keV lines appear to be prompt. It is therefore likely that the isomeric state feeds into the  $12^+$  state, possibly by an unobserved low-energy transition which would explain the isomeric nature.

No transitions associated with  $^{204}\text{Rn}$  were observed in focal plane  $\gamma$ -ray detectors. This would indicate that there are no strongly populated isomers with half-lives longer than  $\sim 0.5 \mu\text{s}$ .

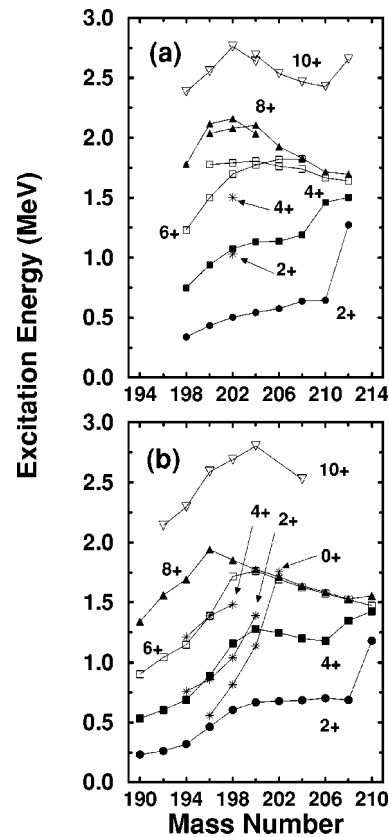


FIG. 16. Systematics of the low-lying yrast states in (a) neutron-deficient radon isotopes and (b) polonium isotopes. The states in different isotopes which are joined by a line in (a) are part of similar decay sequences. Some low-spin nonyrast states are also shown by the asterisks. Sequences are labeled by the spin parity of the states concerned and a common symbol is used for all yrast states of the same spin parity.

## V. INTERPRETATION AND CONCLUSIONS

The low-lying near-yrast states in the light radon isotopes below the  $N=126$  shell closure are illustrated in Fig. 16(a). The data shown are those of Refs. [16–18,25,28–31] along with the results obtained in the current study which complete the systematics by providing a full picture of states up to spin 10 in the  $A=200–204$  nuclides. The proximity of the  $N=126$  and  $Z=82$  shell closures might suggest that the description of nuclei in this region lends itself to a shell model approach. For example, measurements of the magnetic moments of the isomeric  $8_1^+$  states in  $^{206-214}\text{Rn}$  [32], have confirmed the assignment of a proton  $h_{9/2}^4$  configuration. Empirical calculations have been attempted with some success in  $^{208}\text{Rn}$  and heavier isotopes [29–31], albeit using a rather restricted model space and weak coupling between protons and neutrons. Such calculations rapidly become intractable in lighter systems where the increasing number of valence particles dramatically increase the size of the model space. A cursory glance at the energy level systematics shown in Fig. 16(a) shows that the spacing of the  $2^+$ ,  $4^+$ , and  $6^+$  states is roughly equal in the middle of the isotopes shown, which is indicative of vibrational effects. These are clearly anharmonic, as might be expected from coupling of harmonic vi-

brations to an underlying single-particle structure. Such collectivity is indicated by the importance of neutron admixtures into the  $2_1^+$  and  $4_1^+$  states in  $^{206-210}\text{Rn}$  [30]. The interacting boson approximation (IBA-1) has been used to describe states in  $^{206,208}\text{Rn}$  [28], but even these calculations do not reproduce some of the details seen. The fall in the energies of the low-lying states in the lightest isotopes has been linked with the presence of deformed intruder states [18] as discussed in more detail below. The structure of the nuclei studied here is clearly complex and transitional in nature.

Some of these features have been addressed by calculations of Zemel and Dobes [33], who have used the interacting boson model coupled to two-quasiparticle excitations (IBA+QP) to calculate the properties of excited states of spin 2 to 8 in  $^{200-210}\text{Po}$ ,  $^{202-212}\text{Rn}$ , and  $^{204-214}\text{Ra}$ . Data were only available for the polonium isotopes and  $^{204-212}\text{Rn}$  when these calculations were performed, but a reasonable agreement was obtained. The current data allow an extension of the comparison to  $^{202}\text{Rn}$ . The general trend in the IBA+QP predictions is of gradually falling  $2_1^+$  and  $4_1^+$  states with increasing neutron deficiency, corresponding to structures primarily of an IBA collective nature. The calculations reproduce some irregularity in the  $4^+$  systematics nearer the shell closure due to competition between quasiproton and neutron excitations. The  $6^+$  and  $8^+$  states are predicted to rise with falling mass and are dominated by  $\pi h_{9/2}^4$  structures. The data for  $^{202}\text{Rn}$  for  $2_1^+$ ,  $4_1^+$ , and  $8_1^+$  states all agree with these predictions, surprisingly to within a few tens of keV, given the rather limited quasiparticle space used. Due to this restriction the appearance of secondary  $6^+$  and  $8^+$  states is not reproduced; in the lightest nuclei calculated these states are outside of the  $\pi h_{9/2}^+ \nu f_{5/2}$  model space. In an attempt to track states expected to have similar structures, the points in Fig. 16(a) are connected by a straight line if they are part of similar  $\gamma$ -decay pathways; in  $^{202-208}\text{Rn}$  there is a decay path through one set of states populated mainly in the decay of the yrast  $9^-$  state and another not connected with it. The situation in  $^{204}\text{Rn}$  is obviously more complex. Within this scheme, the  $6_2^+$  state in  $^{202}\text{Rn}$  best fits the predicted trends for a  $\pi h_{9/2}^4$  structure but with a reasonable admixture of the IBA collective structure.

For nuclei lighter than  $A=202$ , there is a noticeable fall in the excitation energies of the yrast states. This has been observed previously in the lowest lying states [18]. With the information added in the current work a consistent picture is found of the systematics of states up to spin-10. These systematics indicate the presence of deformed intruder states, which fall in energy as the  $N=82-126$  midshell is approached, by comparison with similar trends in yrast excitation energies in Hg and Pt isotopes below  $Z=82$ . In this latter region, other measured quantities such as transition quadrupole moments and observation of extensive rotational sequences give supporting evidence. The polonium isotopes also display a similar, almost parabolic fall in the excitation energies of states in the lightest systems known. These systematics are shown in Fig. 16(b) for comparison where data has been taken from Ref. [8,9,34–39]. The horizontal axes of

parts (a) and (b) of Fig. 16 have been aligned such that the data point for a particular polonium isotope may be compared directly to the radon isotope which is four mass units heavier. The fall in yrast states in radon isotopes is seen to be very similar in character to the fall observed in the polonium isotopes corresponding to the radon isotopes minus an  $\alpha$  particle. This is suggestive of the effects of  $F$ -spin symmetry, which have been noted in nuclei below the  $Z=82$  shell closure [40] on the basis of the similarity in the relative energies of members of bands built on intruder states. These analog states arise within the context of the interacting boson model where proton and neutron bosons have  $F=\pm\frac{1}{2}$  respectively, and the total  $F$  spin for a state is obtained in a similar way to enumerating the total isospin of a system. In general, ground state  $F$ -spin multiplets are split due to the dependence of the IBA Hamiltonian on  $N_\pi N_\nu$ . However, the formation of intruder configurations by excitation of proton pairs increases the proton boson number, giving larger and more similar  $N_\pi N_\nu$  values within a multiplet. For example, in their ground states  $^{196}\text{Po}$  and  $^{200}\text{Rn}$  should be members of an  $F=4$  multiplet with  $F_0=-3$  and  $-2$ , respectively, but the multiplet is split as  $N_\pi N_\nu$  values are 7 and 12. If intruder states are formed by the excitation in each case of a pair of protons across the  $Z=82$  gap, the intruder configurations form an  $F=5$  multiplet with  $F_0=-2$  and  $-1$ . But now the  $N_\pi N_\nu$  values, 21 and 24, are more equal and the  $F$ -spin symmetry should be consequently better. Detailed analysis of  $F$ -spin analogues in this region is made difficult by the mixing between normal and intruder states, which requires more experimental information to disentangle than is available here. Note that the lightest known  $\alpha$ -pair of Rn and Po isotopes, with masses of 198 and 194, respectively, have  $\gamma$ -ray energies that are fairly similar above the spins where mixing is strong. The pairs of energies for the  $10\rightarrow 8$ ,  $8\rightarrow 6$ , and  $6\rightarrow 4$  are 602/604, 545/548, and 462/481 keV, respectively. In the absence of information which would enable the unperturbed intruder state energies to be extracted, the similarity in the energy systematics is enough to suggest a common mechanism for the intruders in polonium and radon.

A further similarity between polonium and radon isotopes is the appearance of secondary low-spin states. These are marked with asterisks in Fig. 16. Such states were first observed in  $^{196,198}\text{Po}$  isotopes [7], where the in-beam data are supplemented by studies of states populated in  $\alpha$  decay [5], and are interpreted as deformed intruder configurations. In  $^{194}\text{Po}$  there is evidence that such states are a strong mix of spherical and deformed configurations, with the latter assuming the ground-state configuration in lighter isotopes [9,34]. The current work has observed similar nonyrast states in the  $^{198}\text{Po} + \alpha$  nucleus  $^{202}\text{Rn}$ . The predictions of a pairing vibrational model [11] do indicate that the excitation energy of the associated  $0^+$  state should actually be slightly lower in  $^{202}\text{Rn}$  than  $^{198}\text{Po}$ ; the excitation energy of the  $2^+$  states is very similar, but a comparison is complicated by mixing between spherical and deformed configurations and the possibility of slightly different moments of inertia. The observed decay pattern of the states in  $^{202}\text{Rn}$  is slightly different to that in the Po isotopes; the  $2_2^+ \rightarrow 0_{\text{g.s.}}^+$  transition is not observed in the higher energy portion of the spectra in Fig. 9, presumably

due to low efficiency at the expected 1030 keV transition energy combined with low statistics. Low yield has also left the question of the  $E0$  contribution in the transitions to the yrast states open. This component is known to be dependent on the extent of mixing between spherical and deformed configurations and the deformation difference between them [2]. The nonyrast side structures in  $^{204}\text{Rn}$ , such as the state at an excitation energy of 1085 keV may also have a similar origin.

The current work has produced a rather complex level scheme for  $^{204}\text{Rn}$  above spins of  $8\hbar$ . A complete interpretation of these states is difficult, especially in the absence of practicable shell-model calculations. However, some general statements concerning some of the structure can be made, aided by trends in the feeding patterns and configuration assignments from the heavier radon isotopes where schematic calculations have been made [29]. The level scheme of  $^{204}\text{Rn}$  is fragmented and there are many states with similar spins, reflecting the increase in the degrees of freedom with increasing numbers of valence neutron holes in the neutron-deficient isotopes.

A convenient place to begin such discussions is the  $11^-$  state at 2597 keV in  $^{204}\text{Rn}$ . Such states are seen across the radon isotopes with a roughly constant excitation energy and have been attributed to a  $\pi h_{9/2}^3 i_{13/2}$  configuration on the basis of measured  $g$  factors in  $^{208,210}\text{Rn}$  [32]. This level decays to a  $10^-$  state which in  $^{206}\text{Rn}$  [29] has been suggested to be a different coupling of the same configuration. In  $^{206}\text{Rn}$  it decays largely to the yrast  $8^+$  state via an energetic  $M2$  transition and partly to a  $10^+$  state and the yrast  $9^-$  state. Such interpretations of the  $10^-$  and  $11^-$  states seem plausible also in  $^{204}\text{Rn}$ . The  $10^-$  state is isomeric in  $^{204}\text{Rn}$  with a half-life of around 33 ns and it decays via an  $M1$  transition to the yrast  $9^-$  state.  $M2$  transitions to the two  $8^+$  states are not observed, presumably due to the lower transition energies compared to  $^{206}\text{Rn}$  and possibly different wavefunctions of those states (see discussion below) in  $^{204}\text{Rn}$ . There is a  $10^+$  state below the  $10^-$  level but the energy difference is only 10 keV inhibiting that decay path. The only observed decay to the  $9^-$  state must be via a retarded  $M1$  transition. The yrast  $9^-$  level in the heavier isotopes has been associated with a two-quasineutron excitation ( $\nu f_{5/2}^{-1} i_{13/2}^{-1}$ ) which therefore fits with this scenario of a hindered decay path, explaining the isomerism.

The increasing role of neutron degrees of freedom is the likely explanation for the appearance of the pairs of  $6^+$  and  $8^+$  states in  $^{204}\text{Rn}$ , before the intruding deformed  $6^+$  and  $8^+$  states fall in energy in lighter nuclei. In heavier isotopes the yrast states are associated with recoupling the valence proton configuration  $\pi h_{9/2}^4 |_{\nu=2}$ . The  $6^+$  and  $8^+$  states from this configuration rise with neutron deficiency, as seen in the Fig. 16 and the results of Ref. [33], and it is therefore not surprising that neutron configurations eventually become competitive. The decay of the  $9^-$  state, which feeds both  $8^+$  states with almost equal branching, indicates that the wavefunctions of these states are no longer simple in  $^{204}\text{Rn}$ . On the basis of the decay via the 604- and 583-keV transitions, the  $10^+$  states at 2637 and 2688 keV must be candidates for

carrying significant amplitudes of the  $\pi h_{9/2}^4 |_{\nu=4}$  configuration. The other near-yrast  $10^+$  state at 2453 keV, mentioned above, has only one observable decay path via a 234-keV transition to the  $9^-$  state; this probably indicates a structure involving neutron configurations. In  $^{200,202}\text{Rn}$ , the  $9^-$  state feeds only one  $8^+$  state which would tend to indicate that this pathway involves  $6^+$  and  $8^+$  states based on a  $\pi h_{9/2}^4 |_{\nu=2}$ . The other  $6^+$  and  $8^+$  states in  $^{200,202}\text{Rn}$  therefore have some other structure and may be associated with deformed intruders as discussed above.

The  $\mu\text{s}$  isomers in  $^{200,202}\text{Rn}$  have been helpful in determining the level schemes, but it is interesting to ponder on their nature. It is likely, from the little that is known about their feeding pattern, that they have spins of at least  $10\hbar$ . There is indirect evidence that a similar isomer is also present in  $^{198}\text{Rn}$  [18], but in the heavier even-even isotopes there is a single example of a high-spin, long-lived isomer, namely, the 1.6  $\mu\text{s}$   $17^-$  isomer in  $^{210}\text{Rn}$ . Given that the multiplicity of observed purely delayed transitions is small, the spins of the  $^{200,202}\text{Rn}$  isomers are unlikely to be that high. One possibility concerns the  $11^-$  states discussed above. Empirical shell model calculations in  $^{208}\text{Rn}$  actually predict that the  $10^-$  state should lie higher than the  $11^-$  state [29]. These two levels are actually within 140 keV of each other in  $^{204,206}\text{Rn}$ . It is therefore possible that the ordering of these two levels may switch in lighter isotopes, or that they might be separated by only a few tens of keV in  $^{202}\text{Rn}$  and lighter. A situation could easily arise where the decay of the  $11^-$  state by three possible routes. One via an  $E2$  to the  $9^-$  state, retarded by the difference in structure. Another via a low energy transition to the  $10^-$  state with a consequently small transition probability. And finally via an  $E3$  transition to  $8^+$  state with large amplitudes of the  $\pi h_{9/2}^4 |_{\nu=2}$  configuration. The  $8^+$  and  $9^-$  states are certainly populated in the observed isomer decays in  $^{200,202}\text{Rn}$ . This scenario is very similar to that of the  $11^- \pi h_{9/2}^3 i_{13/2}$  states in the light polonium isotopes. Here the observed decays are similar, involving the  $E3$  and retarded  $E2$  transitions. Despite known admixtures of octupole vibrations into the wave function [35], the half-lives of these states increase with neutron deficiency, in the main due to the rising  $8^+$  excitation energy and the  $E_\gamma^7$  transition-probability dependence. In recent measurements of  $^{194}\text{Po}$ , the half-life of the  $11^-$  state is 15  $\mu\text{s}$  [9,34], comparable to that encountered in these radon isotopes. The lack of adequate numbers of  $\gamma$ - $\gamma$  focal plane events frustratingly hampers the determination of the exact isomer decay path, without which the above description of the isomerism must remain speculative. However, candidate transitions in the decays from the  $11^-$  and  $10^-$  states to the  $9^-$  level in  $^{200}\text{Rn}$  are the delayed 183- and 161-keV transitions, giving a 21-keV separation. The lack of observation of a 369-keV  $E3$  transition may suggest that the octupole enhancements seen in polonium isotopes do not extend to radon nuclei, or that the scenario presented here is incorrect. Corresponding candidates in  $^{202}\text{Rn}$  are the delayed 149- and 111-keV transitions, with a 38 keV  $11^-$  to  $10^-$  energy separation.

In summary, knowledge of the decay schemes of  $^{200,202,204}\text{Rn}$  have been extended adding to the picture of the

development of the structure of the neutron-deficient, even-even radon isotopes. The energy systematics of the low-lying states suggest the presence of intruder states which fall with increasing neutron deficiency in a similar way to the polonium isotopes, indicating a common mechanism for the onset of deformation above  $Z=82$ . Candidates have been found for nonyrast intruder states in  $^{202}\text{Rn}$ . The higher-spin levels in the lighter radon isotopes reflect the increasing importance of neutron-hole excitations. Long-lived isomers in  $^{200,202}\text{Rn}$  may be produced by a similar mechanism responsible for the  $11^-$  isomers in the light polonium isotopes. The data on  $^{200,202}\text{Rn}$  also illustrate some of the difficulties of making spectroscopic measurements beyond simple singles  $\gamma$ -ray spectra in the submillibarn regime.

## ACKNOWLEDGMENTS

This work was supported by the U.K. Engineering and Physical Sciences Research Council (EPSRC), the Academy of Finland under the Finnish Centre of Excellence Programme 2000–2005 (Project No. 44875) and by the European Union 5th Framework Programme “Improving Human Research Potential - Access to Research Infrastructure” (HPRI-CT-1999-00044). A.K. was supported by Grant No. HPMF-CT-2000-01115. D.D., A.N.Q., and S.D.R. acknowledge financial support from EPSRC. The authors would also like to thank the U.K.-France Detector Loan Pool for provision of germanium detectors.

- 
- [1] J.L. Wood, K. Heyde, W. Nazarewicz, M. Huyse, and P. Van Duppen, *Phys. Rep.* **215**, 101 (1992).
- [2] J.L. Wood, E.F. Zganjar, C. De Coster, and K. Heyde, *Nucl. Phys.* **A651**, 323 (1999).
- [3] J. Wauters, P. Dendooven, M. Huyse, G. Reusen, P. Lievens, P. Van Duppen, and the ISOLDE Collaboration, *Z. Phys. A* **344**, 29 (1992).
- [4] J. Wauters, N. Bijmens, P. Dendooven, M. Huyse, H.Y. Hwang, G. Reusen, J. von Schwarzenberg, P. Van Duppen, R. Kirchner, E. Roeckl, and the ISOLDE Collaboration, *Phys. Rev. Lett.* **72**, 1329 (1994).
- [5] N. Bijmens, P. Decrock, S. Franchoo, M. Gaelens, M. Huyse, H.-Y. Hwang, I. Reusen, J. Szerypo, J. von Schwarzenberg, J. Wauters, J.G. Correia, A. Jokinen, P. Van Duppen, and the ISOLDE Collaboration, *Phys. Rev. Lett.* **75**, 4571 (1995).
- [6] N. Bijmens, P. Decrock, S. Franchoo, M. Gaelens, M. Huyse, H.-Y. Hwang, I. Reusen, J. Szerypo, J. von Schwarzenberg, G. Vancraeynest, P. Van Duppen, and J. Wauters, *Phys. Rev. C* **58**, 754 (1998).
- [7] D. Alber, R. Alfier, C.E. Bach, D.B. Fossan, H. Grawe, H. Kluge, M. Lach, K.H. Maier, M. Schramm, R. Schubart, M.P. Waring, L. Wood, H. Hubel, and J.-Y. Zhang, *Z. Phys. A* **339**, 225 (1991).
- [8] L.A. Bernstein, J.A. Cizewski, H.-Q. Jin, W. Younes, R.G. Henry, L.P. Farris, A. Charos, M.P. Carpenter, R.V.F. Janssens, T.L. Khoo, T. Lauritsen, I.G. Bearden, D. Ye, J.A. Becker, E.A. Henry, M.J. Brinkman, J.R. Hughes, A. Kuhnert, T.F. Wang, M.A. Stoyer, R.M. Diamond, F.S. Stephens, M.A. Deleplanque, A.O. Macchiavelli, I.Y. Lee, B. Cederwall, J.R.B. Oliveira, J. Burde, P. Fallon, C. Duyar, J.E. Draper, E. Rubel, and D.T. Vo, *Phys. Rev. C* **52**, 621 (1995).
- [9] K. Helariutta, J.F.C. Cocks, T. Enqvist, P.T. Greenlees, P. Jones, R. Julin, S. Juutinen, P. Jämsen, H. Kankaanpää, H. Kettunen, P. Kuusiniemi, M. Leino, M. Muikku, M. Piiparinen, P. Rakhila, A. Savelius, W.H. Trzaska, S. Törmänen, J. Uusitalo, R.G. Allatt, P.A. Butler, R.D. Page, and M. Kapusta, *Eur. Phys. J. A* **6**, 289 (1999).
- [10] W. Younes and J.A. Cizewski, *Phys. Rev. C* **55**, 1218 (1997).
- [11] A.M. Oros, K. Heyde, C. De Coster, B. Decroix, R. Wyss, B.R. Barrett, and P. Navratil, *Nucl. Phys.* **A645**, 107 (1999).
- [12] E. Marshalek, L. Person, and R.K. Sheline, *Rev. Mod. Phys.* **35**, 108 (1963).
- [13] P. Möller and J.R. Nix, *At. Data Nucl. Data Tables* **26**, 165 (1981).
- [14] R. Bengtsson, P. Möller, J.R. Nix, and J. Zhang, *Phys. Scr.* **29**, 402 (1984).
- [15] P. Möller and J.R. Nix, and W.J. Swiatecki, *At. Data Nucl. Data Tables* **59**, 185 (1995).
- [16] S.J. Freeman, A.G. Smith, S.J. Warburton, B.B. Back, I.G. Bearden, D.J. Blumenthal, M.P. Carpenter, B. Crowell, C.N. Davids, D. Henderson, R.V.F. Janssens, T.L. Khoo, T. Lauritsen, C.J. Lister, D. Nisius, H.T. Penttila, J.A. Becker, P. Chowdhury, and E.F. Moore *Phys. Rev. C* **50**, 1754 (1994).
- [17] R.B.E. Taylor, S.J. Freeman, J.L. Durell, M.J. Leddy, A.G. Smith, D.J. Blumenthal, M.P. Carpenter, C.N. Davids, C.J. Lister, R.V.F. Janssens, and D. Seweryniak, *Phys. Rev. C* **54**, 2926 (1996).
- [18] R.B.E. Taylor, S.J. Freeman, J.L. Durell, M.J. Leddy, S.D. Robinson, J.F.C. Cocks, J.F.C. Cocks, K. Helariutta, P. Jones, R. Julin, S. Juutinen, H. Kankaanpää, A. Kanto, H. Kettunen, P. Kuusiniemi, M. Leino, M. Muikku, P. Rakhila, and A. Savelius, *Phys. Rev. C* **59**, 673 (1999).
- [19] M. Leino, J. Äystö, T. Enqvist, P. Heikkinen, A. Jokinen, M. Nurmia, A. Ostrowski, W.H. Trzaska, J. Uusitalo, K. Eskola, P. Armbruster, and V. Ninov, *Nucl. Instrum. Methods Phys. Res. B* **99**, 653 (1995).
- [20] P.J. Nolan, F.A. Beck, and D.B. Fossan, *Annu. Rev. Nucl. Part. Sci.* **45**, 561 (1994).
- [21] P.J. Nolan, D. Gifford, and P.J. Twin, *Nucl. Instrum. Methods Phys. Res. A* **236**, 95 (1985).
- [22] M. Moszyński, J.H. Bjerregard, J.J. Gaardhøje, B. Herskind, P. Knudsen, and G. Sletten, *Nucl. Instrum. Methods Phys. Res. A* **280**, 73 (1989).
- [23] F. Calaprice, G.T. Ewan, R.-D. von Dincklage, B. Jonson, O.C. Jonsson, and H.L. Ravn, *Phys. Rev. C* **30**, 1671 (1984).
- [24] G. Palameta and J.C. Waddington, *Nucl. Instrum. Methods* **234**, 476 (1985).
- [25] D. Horn, C. Baktash, and C.J. Lister, *Phys. Rev. C* **24**, 2136 (1981).
- [26] A.N. Qadir, Ph.D. thesis, University of Manchester, 2001.

- [27] K.S. Krane, R.M. Steffen, and R.W. Wheeler, Nucl. Data Tables **11**, 351 (1973).
- [28] B.G. Ritchie, F.T. Avignone III, H.K. Carter, R.L. Mlekodaj, and E.H. Spejewski, Phys. Rev. C **23**, 1717 (1981).
- [29] W.J. Triggs, A.R. Poletti, G.D. Dracoulis, C. Fahlander, and A.P. Byrne, Nucl. Phys. **A395**, 274 (1983).
- [30] A.R. Poletti, G.D. Dracoulis, C. Fahlander, and I. Morrison, Nucl. Phys. **A380**, 335 (1982).
- [31] G.D. Dracoulis, P.M. Davidson, A.P. Byrne, B. Fabricius, T. Kibedi, A.M. Baxter, A.E. Stuchbery, A.R. Poletti, and K.J. Schiffer, Phys. Lett. B **246**, 31 (1990).
- [32] K.H. Maier, D.J. Decman, H. Grawe, H. Haas, and W.-D. Zeitz, Hyperfine Interact. **9**, 87 (1981), and references therein.
- [33] A. Zemel and J. Dobes, Phys. Rev. C **27**, 2311 (1983).
- [34] R. Julin, K. Helariutta and M. Muikku, J. Phys. G **27**, 109 (2001).
- [35] A. Maj, H. Grawe, H. Kluge, A. Kuhnert, K.H. Maier, J. Recht, and N. Roy, Z. Phys. A **324**, 123 (1986).
- [36] B. Fant, T. Wreckström and A. Källberg, Phys. Scr. **41**, 652 (1990).
- [37] A.M. Baxter, A.P. Bryne, G.D. Dracoulis, R.A. Bark, F. Riess, A.E. Stuchbery, M.C. Kruse, and A.R. Poletti, Nucl. Phys. **A515**, 493 (1990).
- [38] A.R. Poletti, G.D. Dracoulis, A.P. Bryne, A.E. Stuchbery, B. Fabricius, T. Kibedi, and P.M. Davidson, Nucl. Phys. **A615**, 95 (1997).
- [39] E. Browne and R.B. Firestone, in *Table of Radioactive Isotopes*, edited by V.S. Shirley (Wiley, New York, 1986).
- [40] B.R. Barrett, G.D. Dracoulis, and R.A. Bark, Phys. Rev. C **43**, 926 (1991).